On the Nature of Super-Resolution in Inverse Scattering*

Alaeddin A. Aydıner, Weng Cho Chew
Center for Computational Electromagnetics and Electromagnetic Laboratory
Department of Electrical and Computer Engineering
University of Illinois at Urbana-Champaign

Abstract

This work studies the nature of super-resolution, the phenomenon of resolution beyond the diffraction limit, which has been experimentally and numerically verified for acoustic and electromagnetic waves. The prospect of subwavelength resolution at optically large observation distances is investigated. Two conjectures as to how super-resolution can be attained are evaluated and tested. The first conjecture underscores the unraveling of the phase accumulations during multiple scattering of propagating waves whereas the second relies on the conversion of evanescent spectrum to propagating waves that can be observed at the far-field.

I Introduction

Super-resolution is a curious nonlinear inverse scattering phenomenon which enables us to resolve objects far smaller than the wavelength used to probe them. Since the early 90's, it has been demonstrated through experiments and numerical simulations not only in the electromagnetic realm [1–5] but also in the acoustic realm [6–8]. A better understanding of super-resolution may lead to major advances in nondestructive testing, remote sensing and in the inverse algorithms themselves as discussed briefly in the conclusions. However, to the authors' knowledge, such a study has not been undertaken, mainly owing to its nonlinear nature which precludes an analytical approach. This nonlinearity is mainly due to multiple scattering. Hence, it is essential to understand the effects of multiple scattering in order to understand super-resolution, but the former can be analyzed mainly through numerical simulations. In this work, we assume the 2D TM problem governed by the scalar wave equation to facilitate insight into the phenomenon. We also assume the $e^{-i\omega t}$ time-dependence and that no *a priori* information is available concerning the location and contrast of the objects to be reconstructed.

We define the diffraction limit, also called the Rayleigh criterion, to be $\lambda/4$ rather than the widely assumed $\lambda/2$. This is because the scattered field E_z can be expressed as the Fourier transform of the object or contrast function $O(\boldsymbol{\rho}') = k^2(\boldsymbol{\rho}') - k_o^2$ with the Born and far-field approximations [9]:

$$E_z \sim \int d\boldsymbol{\rho}' e^{-(\boldsymbol{k_r}-\boldsymbol{k_t})\cdot\boldsymbol{\rho}'} O(\boldsymbol{\rho}'). \tag{1}$$

Here, $\boldsymbol{k_r} = k_o\hat{\rho}_r$ and $\boldsymbol{k_t} = -k_o\hat{\rho}_t$ are related to the receiver and transmitter positions denoted by $\hat{\rho}_r$ and $\hat{\rho}_t$ respectively. By the Nyquist criterion, variations in the object function can happen only if

$$\Delta\rho' > \frac{\pi}{\max|\boldsymbol{k_r} - \boldsymbol{k_t}|} = \frac{\lambda}{4} \tag{2}$$

where we assume that $k_r = k_t = k_o = 2\pi/\lambda$. Thus, with a suitable receiver-transmitter configuration, quarter wavelength resolution can be achieved by diffraction tomography alone.

The two possibly corroborating conjectures that will be tested in this study are:

1. Propagating waves undergo multiple scattering within subwavelength distances and hence accumulate a phase that is a function of such distances. The unraveling of these phase effects by an inverse solver lies behind super-resolution. Indeed, there are even reconstruction schemes such as [10] that rely on the unwrapping of phase.

2. The evanescent near-field spectrum undergoing multiple scattering is converted into propagating waves. Thus, the far-field pattern contains much higher spectral content, albeit in disguise.

*This work was supported by Department of Energy grant DOE DEFG07-97ER 14835 and Air Force Office of Scientific Research under MURI grant F49620-96-1-0025.

0-7803-7846-6/03/$17.00 ©2003 IEEE

II Formulation and Results

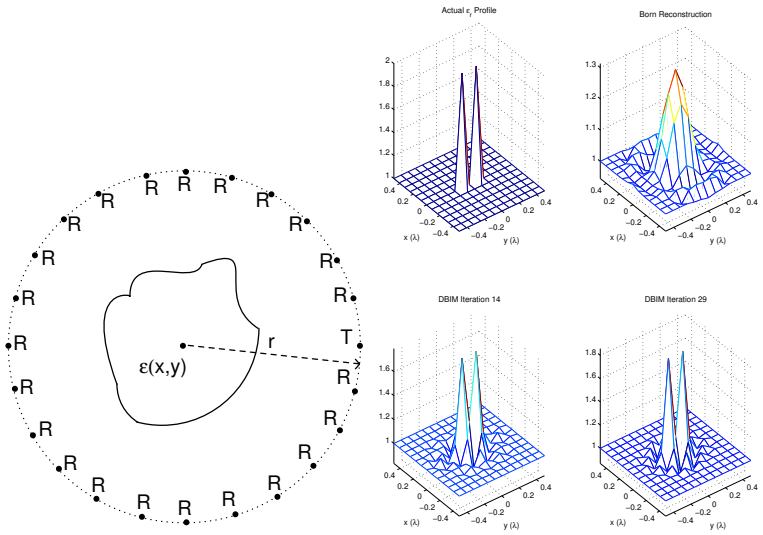

(a) (b)

Figure 1: (a) TX/RX configuration. (b) Reconstructions for the $r = 2048\lambda$ case.

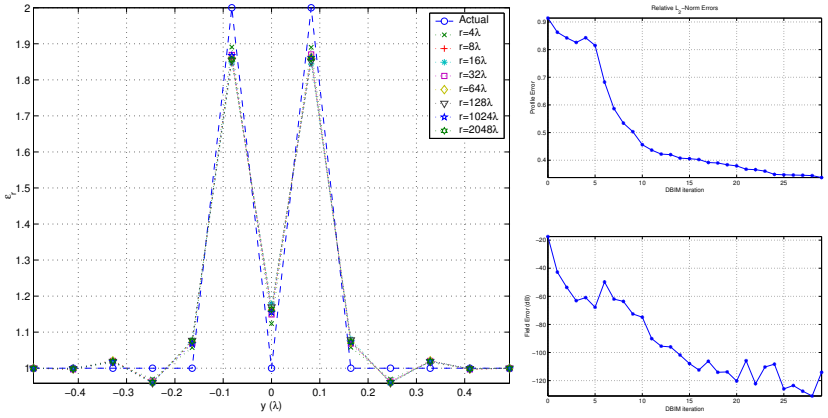

(a) (b)

Figure 2: (a) The super-resolved crossection for various r. (b) DBIM convergence for the $r = 2048\lambda$ case. Relative L_2-norm is defined by $\sqrt{\sum_n |f_n - f_n^e|^2 / \sum_n |f_n^e|^2}$ where the superscript e stands for "exact".

We use the setup in Figure 1-a with 8 transmitters and 32 receivers distributed over a circle of radius r meters surrounding the computational domain. The discretization and domain sizes in terms of the wavelength are shown in Figure 1-b. The algorithm used in the inversion is the distorted Born iterative method (DBIM) [11]. The radiating, incident and backpropagating Green's functions are scaled by $\sqrt{r}$ to render the regularization procedure independent of observation distance. The inverse problem is Tikhonov-regularized by an identity matrix scaled by a regularization factor γ, which is gradually decreased to a minimum to allow for higher spectral content with each iteration. The *only* difference among the reconstructions in Figure 2-a is the observation distance r. The two single pixel, i.e., 0.082λ x 0.082λ, objects are separated by only 0.082λ. Here, we note that the contrast in Figure 2 is actually expanded in

terms of pulses. In each case, the $29th$ iteration is shown where the scattered field error is around -120 dB. The reconstructions cannot achieve the perfect profile because the field difference is about -100 dB by the $14th$ iteration.

As shown in the Appendix, the evanescent waves are buried in the irregular part of the Hankel function, i.e., the Neumann function, which has spectral contents far above the wavenumber k_o. Hence, a purely propagating Green's function results if we adopt the Bessel function as the Green's function. In the setting of a simple (pulse basis, point matching) method of moments implementation, this would lead to the following modification of the Green's function utilized in the computation of the *internal* field:

$$\int\int_{S_i} G(\boldsymbol{\rho}_j - \boldsymbol{\rho}')\, dx'\, dy' = \begin{cases} \frac{i}{4} H_o^{(1)}(k_o \rho_{mn}) \Delta x \Delta y & m \neq n \\ \frac{i}{2k_o^2}\left[\pi k_o\, a H_1^{(1)}(k_o\, a) + 2i\right] & m = n \end{cases} \Rightarrow \begin{cases} \frac{i}{4} J_o(k_o \rho_{mn}) \Delta x \Delta y & m \neq n \\ \frac{i}{2k_o} \pi a J_1(k_o\, a) & m = n \end{cases} \tag{3}$$

where $a = \sqrt{\Delta x\, \Delta y/\pi}$ and $\rho_{mn} = \sqrt{(x_m - x_n)^2 + (y_m - y_n)^2}$.

With the above change of the *internal* Green's function, there is surprisingly little difference in the scattered fields as shown in Figure 3-a. Here, the various curves are due to incident fields from the 8 transmitters, some of which overlap. Although the resulting inversion converges, it fails to resolve the two distinct objects as shown in Figure 3-b .

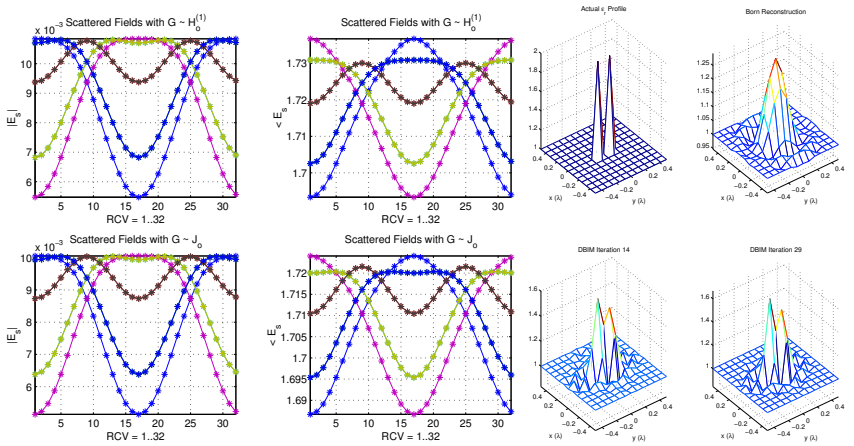

(a) (b)

Figure 3: (a) The scattered fields due to the Bessel Green's function as the internal Green's function are quite similar to those due to the actual Hankel one. (b) DBIM fails to reconstruct the objects distinctly without evanescent fields.

III Conclusions

With sufficiently high signal-to-noise ratio equipment, it should be possible to observe super-resolution at optically large distances. This can lead to advances in e.g. medical imaging where the equipment should be as unintrusive as possible. The imperfect reconstructions result because the field difference is minimized to a level close to the numerical noise floor.

It has been shown that evanescent waves play a vital role in the super-resolution of objects.

Super-resolution cannot be readily demonstrated by all inverse scattering algorithms. For example, it is known in general that the first-order Born iterative method (BIM) cannot perform as well as the second-order DBIM [2], and that at least one gradient based approach fails to achieve super-resolution without *a priori* information concerning the location of the object [1]. The correlation of backpropagated or time-reversed received fields with the currents in the computational domain may be a prerequisite to the manifestation of super-resolution [7]. Such correlations are performed by the (D)BIM algorithms when the functional to optimize is solved since conjugate transpose of the

inverse operator, which corresponds to backpropagated or time-reversed fields in the time-domain, appears in the solution. Future research is necessary to elicit these points.

IV Appendix

In the spectral domain, the 2D Green's function can be expressed as

$$G(\boldsymbol{\rho}, \boldsymbol{\rho}') = \frac{i}{4} H_o^{(1)}(k_o \rho) = \frac{i}{4\pi} \int_{-\infty}^{\infty} dk_x \frac{e^{i(k_x x + k_y |y|)}}{k_y} \tag{4}$$

where $k_y = \sqrt{k_o^2 - k_x^2}$ [12]. By virtue of the dispersion relation, $k_o^2 = k_x^2 + k_y^2$, waves evanesce in the y-direction while propagating in the x-direction. Hence, in general, the designation of evanescence or propagation depends on the coordinate system. However, the regular part of the Hankel function, i.e., the Bessel function, is free of evanescent waves, regardless of how the coordinate system is rotated. That is,

$$H_o^{(1)}(k_o \rho) = \int_{-\infty}^{\infty} dk_x \frac{e^{i(k_x x + k_y |y|)}}{k_y} = \int_0^{\infty} dk_x \, \cos(k_x x) \frac{e^{i k_y |y|}}{k_y} \tag{5-a}$$

$$= \int_0^{k_o} dk_x \, \cos(k_x x) \frac{e^{i k_y |y|}}{k_y} + \int_{k_o}^{\infty} dk_x \, \cos(k_x x) \frac{e^{-|k_y||y|}}{i|k_y|} \tag{5-b}$$

in which the purely imaginary second integral on the right-hand side contains all the evanescent spectrum. Therefore, taking the real part of both sides of the equation reveals that $J_o(k_o \rho)$ is free of evanescent waves.

References

[1] M. Moghaddam and W. C. Chew, "Comparison of the born iterative method and Tarantola's method for an electromagnetic time-domain inverse problem," *International Journal of Imaging Systems and Technology*, vol. 3, pp. 318–333, Winter 1991.

[2] Y. M. Wang and W. C. Chew, "Accelerating the iterative inverse scattering algorithms by using the fast recursive aggregate T-matrix algorithm," *Radio Science*, vol. 27, pp. 109–116, Mar. 1992.

[3] D. Courjon and C. Bainier, "Near-field microscopy and near-field optics," *Reports on Progress in Physics*, vol. 57, pp. 989–1028, Oct. 1994.

[4] J.-J. Greffet, A. Sentenac, and R. Carminati, "Surface profile reconstruction using near field data," *Optics Communications*, vol. 116, pp. 20–24, Apr. 1995.

[5] F.-C. Chen and W. C. Chew, "Experimental verification of superresolution in nonlinear inverse scattering," *Applied Physics Letters*, vol. 72, pp. 3080–3082, June 1998.

[6] J. de Rosny and M. Fink, "Overcoming the diffraction limit in wave physics using a time-reversal mirror and a novel acoustic sink," *Physical Review Letters*, vol. 89, Sept. 2002.

[7] P. Blomgren, G. Papanicolaou, and H. Zhao, "Super-resolution in time-reversal acoustics," *Journal of the Acoustical Society of America*, vol. 111, pp. 230–248, Jan. 2002.

[8] M. Moghaddam and W. C. Chew, "Simultaneous inversion of compressibility and density in the acoustic inverse problem," *Inverse Problems*, vol. 9, pp. 715–730, Dec. 1993.

[9] W. C. Chew, *Waves and Fields in Inhomogeneous Media*. IEEE Electromagnetic Series, New York: IEEE Press, 2nd ed., 1995.

[10] P. M. Meaney, K. D. Paulsen, B. W. Pogue, and M. I. Miga, "Microwave image reconstruction utilizing log-magnitude and unwrapped phase to improve high-contrast object recovery," *IEEE Transactions on Medical Imaging*, vol. 20, pp. 104–116, Feb. 2001.

[11] W. C. Chew and Y. M. Wang, "Reconstruction of two-dimensional permittivity distribution using the distorted born iterative method," *IEEE Transactions on Medical Imaging*, vol. 9, pp. 218–225, June 1990.

[12] M. Abramowitz and I. A. Stegun, *Handbook of Mathematical Functions*. New York: Dover Publications, 1972.